ARTICLE

Vacancy Clusters in Graphane as Quantum Dots

Abhishek K. Singh, Evgeni S. Penev, and Boris I. Yakobson*

Department of Mechanical Engineering and Materials Science and Department of Chemistry, Rice University, Houston, Texas 77005

ABSTRACT Complementary electronic properties and a tendency to form sharp graphene—graphane interfaces open tantalizing possibilities for two-dimensional nanoelectronics. First-principles density functional and tight-binding calculations show that graphane can serve as natural host for graphene quantum dots, clusters of vacancies in the hydrogen sublattice. Their size n, shape, and stability are governed by the aromaticity and interfaces, resulting in formation energies $\sim 1/\sqrt{n}$ eV/atom and preference to hexagonal clusters congruent with lattice hexagons (*i.e.*, with armchair edge). Clusters exhibit large gaps $\sim 15/\sqrt{n}$ eV with size dependence typical for confined Dirac fermions.

KEYWORDS: nanoelectronics · graphane · graphene · quantum dots · interfaces

Electron confinement in one or more dimensions is a powerful way to change materials physics for applications. Quantum dots (QDs) represent an extreme where complete confinement leads to often desired atom-like electronic properties.[1] Major advantage of QDs is the tunability of their optoelectronics, controlled by size, shape, composition, and strain, which together define the confinement potential of electrons and holes. Recently discovered graphene[2] has attracted interest as a natural realization of two-dimensional (2D) carbon crystal,[3] including "cutting" it into nearly 1D nanoribbons.[4] Further confinement toward graphene QDs turns out to be a challenge that triggered intense studies of large graphene dots.[5−9] The larger QDs of graphene hold promise for spintronics,[10] although their small gaps limit optoelectronics applications. Both ribbons and dots suffer from irregular edges and mechanical delicacy,[11] posing a problem for handling and assembly.

As an alternative to ribbons, we have recently discussed *nanoroads*[12]—narrow areas in the hydrogenated graphene (CH, graphane[13,14]) stripped off H. Such graphene roads,[12,15] confined by the fields of graphane as insulating host material,[14,16] show all the properties of broadly discussed ribbons. Yet they remain planar and can, in principle, be connected within the same 2D sheet, without compromising its mechanical integrity. An important evidence of reversible hydrogenation has been recently reported,[17−19] although precise morphology in experiments remains unclear. It is tempting to speculate on a variety of ways to attach H (or perhaps fluorine) to the graphene substrate to form lines, shapes, and patterns, yet analysis shows that most of them are thermodynamically not feasible[20] and can either aggregate into larger CH clusters or simply decompose into H_2 gas. Only more compact, dense islands of coexisting 2D phases, C and CH, are likely to stabilize and be of practical interest.

With this in mind, here we explore a formation of QDs as small islands of graphene in graphane host. Their feasibility is evaluated by systematically computing the energies of numerous configurations, essentially H vacancy aggregates in the underlying CH lattice. This reveals a general trend in the formation energy, $\varepsilon(n) - \varepsilon(\infty) \sim \text{const}/\sqrt{n}$, as a function of QD size n, as well as particular stable vacancy clusters (often corresponding to aromatic molecules). For larger QD islands, it is important to separate the energy of small lattice mismatch ($\sim$2%[14,19]) in order to define the interface energy. It is lower for the armchair (AC) border than for the zigzag (ZZ), suggesting the hexagonal shapes as preferred Wulff constructs. Computed electronic level gaps are large in the small QD and decrease with size n as $E_g \sim 1/\sqrt{n}$, following common confinement trend, but in a way rather characteristic for Dirac fermions.[21]

*Address correspondence to biy@rice.edu.

Received for review March 24, 2010 and accepted May 2, 2010.

Published online May 13, 2010.
10.1021/nn1006072

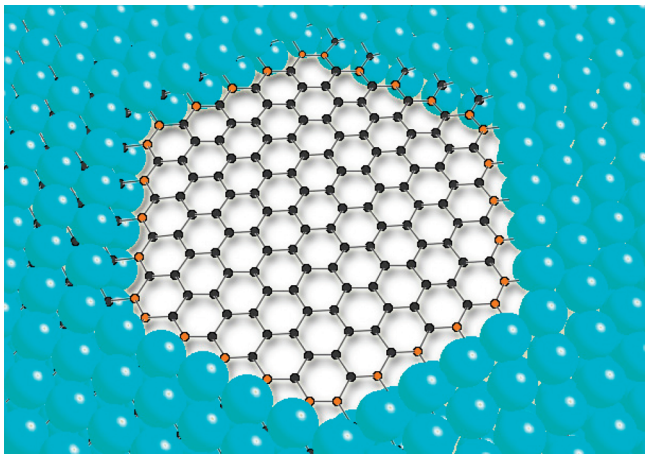

Figure 1. Hexagonal graphene "dot" formed by removing $n = 150$ H atoms (cyan spheres) from a graphane sheet. The ZZ interface sp^2-carbon atoms are highlighted, total $n_{int} = \sqrt{6n} = 30$ of them, bound to sp^3- carbons of graphane.

RESULTS AND DISCUSSION

To evaluate the QD formation energies, we consider a gedanken process of hydrogen removal from a graphane sheet, $(CH)_N \rightarrow (CH)_{N-n}(C)_n + (n/2)H_2$. Only simply connected shapes formed by n atoms of sp^2-carbon are considered as a QD (Figure 1). The formation energy $\varepsilon(n)$ per atom of a vacancy cluster of size n is defined as

$$n\varepsilon(n) = E_{tot}(n) + \mu_H n - \mu_{CH} N \qquad (1)$$

where $E_{tot}(n)$ is the total energy of the system representing the quantum dot, and $\mu_H = (1/2)E_{H_2}$ and μ_{CH} are the chemical potentials of hydrogen and of a CH unit in graphane, respectively (for details, please see the Methods section).

For each cluster size n, we consider several symmetry nonequivalent geometries, typically derived from the lowest-energy shape for $n - 1$. The calculated $\varepsilon(n)$ values are shown in Figure 2. Clearly, all clusters with complete aromatic rings are local minima. The removal of H atom leaves an unfavorable radical behind. Subsequent removal of H from the adjacent C atom leads to formation of an additional π bond between these newly formed sp^2-carbon atoms, lowering the energy significantly. For the dots where the removal results in a benzene-like C configuration, it brings about further stabilization. Thus, the systems here follow the fundamental chemistry of aromatic molecules. QDs of sizes 6, 10, 12, and 24 can be viewed as embedded benzene, naphthalene, pyrene, and coronene, respectively.[22] For $n > 25$, we consider 10 hexagonal shapes (see discussion below) of purely ZZ ($n = 54$, 96, 150, 216, 294, and 384) and AC ($n = 42$, 114, 222, and 366) edges. For example, the optimized structure of a $n = 150$ dot is shown in Figure 1.

While for small n the cluster detail is essential, for large QD, a general trend $\varepsilon(n) - \varepsilon(\infty) \sim \text{const}/\sqrt{n}$ becomes apparent, a manifestation of energy cost of graphene−graphane interfaces γ (indeed, perimeter contribution to the total energy scales as $\sqrt{n}$, and divided by the cluster size n, yields a $1/\sqrt{n}$). Magnitudes

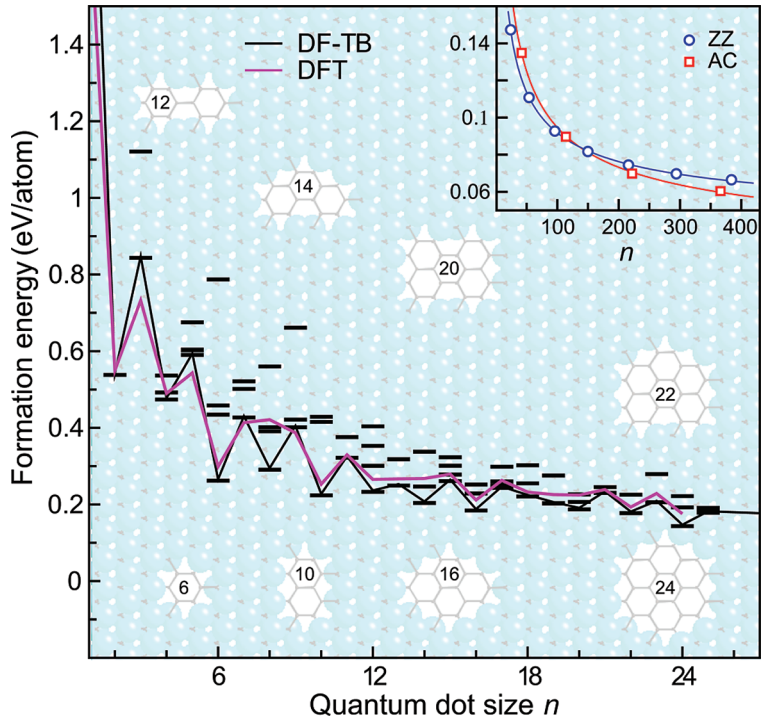

Figure 2. Quantum dot formation energy $\varepsilon(n) - \varepsilon(\infty)$ as a function of the size n. The lowest-energy configurations for each n are connected by a solid line to guide the eye (black for DF-TB, magenta for DFT). Selected low-energy QD shapes are shown in the background. The inset shows the energies of large dots with ZZ and AC borders, calculated with DF-TB.

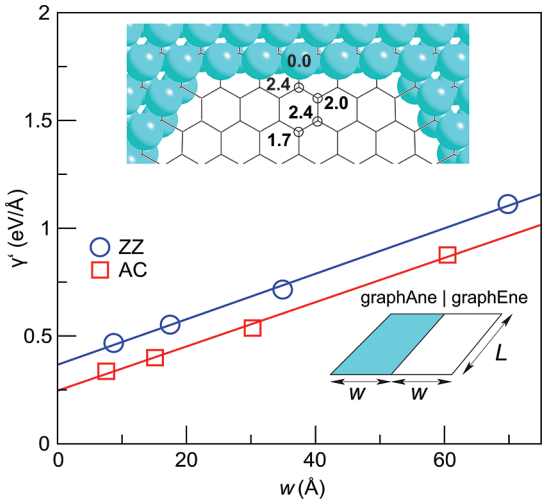

Figure 3. Energy due to graphane−graphene interface (ZZ and AC types) grows with the sample width *w* (geometry schematics are shown in the lower inset). Symbols represent the DF-TB calculated points, solid lines give the linear least-squares regression. The top inset shows the destabilization energies of the interface (in eV) upon H atom displacement to the indicated sites.

of γ are important as it determines the interface stability as well as equilibrium QD shape. Its calculation requires special care as the quantity $E_{tot}(n)$, typically obtained from a supercell computation, contains an elastic strain term caused by the lattice mismatch, which scales linearly with the cell size. We take advantage of this scaling in order to extract the interface energy *per se*. For a supercell consisting of two halves of size $L \times w$ (lower inset in Figure 3), its total energy exceeds the sum of energies of separate phases (CH and C) by

$$E_{tot}(N/2) - (\mu_C + \mu_{CH})N/2 \equiv L\gamma'(w) = L(C\varepsilon^2 w + 2\gamma) \quad (2)$$

with *C* and ε being elastic constant and strain. For both ZZ and AC interfaces, a set of DF-TB calculations is performed for fixed *L* and several sizes 2*w*. In Figure 3, the data actually follow linear dependence very well. Then γ is obtained from the intercept in the linear regression of the computed $\gamma'(w)$. This yields for the ZZ and AC interfaces $\gamma_{ZZ} = 0.18$ eV/Å and $\gamma_{AC} = 0.12$ eV/Å. Note that the slopes for ZZ and AC cases in Figure 3 are identical, in accord with isotropic elasticity of hexagonal 2D crystals.

For a given *n*, the equilibrium shape of a large cluster is determined by minimizing the total interface energy, which results in Wulff construction.[23] For a hexagon, the ratio of distances from its center to a corner and that to a side is $2/\sqrt{3} = 1.155 < \gamma_{ZZ}/\gamma_{AC} = 1.5$. Wulff construction then results in hexagonal clusters with AC edges (with no corner truncation or rounding, which could occur at smaller γ_{ZZ}/γ_{AC} ratios). This orientation preference also agrees with Figure 2, where the large AC dots have lower formation energies. For smaller dots, the shapes deviate from Wulff construction as the corner contributions become dominant.[24]

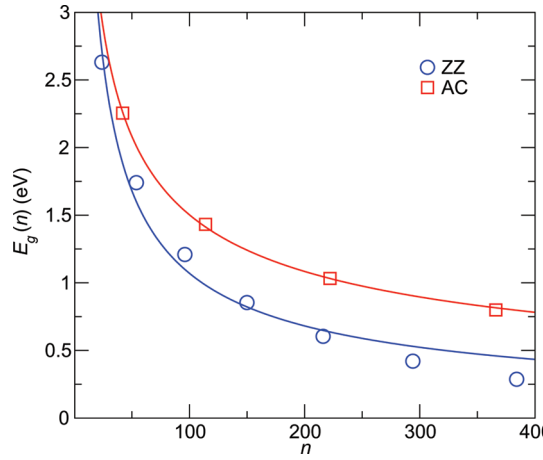

Figure 4. Energy gap $E_g(n)$ as a function of the QD size *n*. Solid curves are least-squares fits.

Lastly, since the QD electronics can be affected by the sharpness of boundaries, we evaluate their robustness by a simple test. We calculate the energy increase upon displacing a single H atom away from the interface as shown in the top inset of Figure 3. The high energy cost for such imperfections, in agreement with our previous work on nanoroads,[12] should support the edge "quality" against disorder and thermal fluctuations.

Next we explore the confinement effect on the electronic properties of these dots. The DF-TB energy gaps E_g at the Γ point are shown in Figure 4. For $n = 6$ and 24 [$E_g(6) = 4.39$ and $E_g(24) = 2.63$ eV], we also compute the highest occupied−lowest unoccupied molecular orbitals (HOMO−LUMO) gaps with DFT [$E_g(6) = 4.02$ eV and $E_g(24) = 2.53$ eV]. The values agree well, lending further credibility to the employed DF-TB parameter set. The results distinctly differ for ZZ and AC edges, with the gaps being always larger in the AC case. Least-square fits give $E_g(n) = 13.2n^{-1/2+0.03}$ eV for AC edges and $E_g(n) = 21.5n^{-1/2-0.15}$ eV for ZZ edges. The gaps decrease with the linear dimension but do not obey the $\sim 1/R^2$ dependence in conventional quantum dots.[1] Instead, the computed trend conforms closer with the confinement of Dirac fermions.[3,8,16] Indeed, the quasiparticle spectrum of large graphene dots is essentially described by the solution to the 2D Dirac equation. In the approximation of circular dot of radius $R \sim \sqrt{n}$ with hard-wall boundary condition,[21] the energy level separation $E_g = \hbar v_F \pi / R$, with v_F being the Fermi velocity of graphene.

As expected, in the limit of very large *n*, the QDs recover the electronic spectrum of graphene, which is studied in great detail.[3] These larger QDs display band gaps of the order of meV, too small for optical applications, yet holding promise for spintronics,[10] as the splitting can be controlled by magnetic field.[8,9] In the optical range, the numerical gap values are important, and one should be reminded that DF-TB as well as DFT computations usually underestimate the gap. In the present case, the system sizes certainly prohibit the use of the

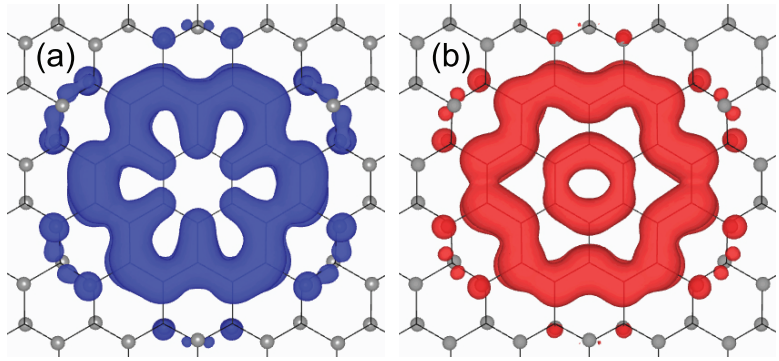

Figure 5. Isosurfaces of band decomposed electron densities (6×10^{-4} Å $^{-3}$) of (a) the top of the valence and (b) the bottom of the conduction bands for a hexagonal QD array with $n = 24$. Note that the "leak" into graphane host material is very small.

computationally expensive GW gap corrections. Recently, Lebègue *et al.*[16] have calculated the optical gap of graphane using the GW approximation and found an underestimation of ≃35% in the DFT results. With this in mind, and on the basis of our analysis, we expect the true optical gaps to reach the range ∼1−3 eV relevant to optoelectronics applications.

Since for optical applications these QDs are usually assembled in 2D arrays, we next study an example assembly of the $n = 24$ size QD using DFT. The dots are arranged in a hexagonal lattice with a 4×4 periodicity of graphane lattice, resulting in a dot−dot separation of ≃7.6 Å. The band gap of such a QD array, $E_g = 2.6$ eV, is very similar to that of an isolated dot. The top of the valence and the bottom of the conduction bands are nearly dispersionless, a feature of atom-like states. These bands are entirely derived from the sp^2-carbon constituting the dots as seen from the corresponding band decomposed charge densities shown in Figure 5. We intentionally show the charge density with low isodensity threshold to detect very small "leakage" into graphane. Clearly, these states are well localized within the QD, confirming that graphane serves well as host material. The larger dots are also expected to show a similar trend that may render them suitable for optical applications.

CONCLUSIONS

In summary, we have demonstrated, by employing DF-TB and DFT calculations, the suitability of graphane as a host for graphene QD. We have found that the shape and size of such dots depend crucially on the graphene/graphane interface energy and the degree of aromaticity. Furthermore, these graphene dots show a pronounced quantum confinement effect of Dirac fermions, with energy gaps lying in the optically relevant range. Given the recent progress on hydrogenation of graphene,[19,25] we believe that the possibility presented here may become part of the experimental development in the field of carbon-based nanoelectronics.

METHODS

The total energies for $n = 1-384$ were calculated using density functional theory based tight-binding (DF-TB) method as implemented in the DFTB+ code[26] and the associated Slater−Koster parameters.[27] The host graphane is represented by a supercell of nearly square shape with $N = 836$. Periodic boundary conditions are imposed in all three dimensions. The lateral box size is set to $(L_x,L_y) = (p|\mathbf{a}_1|, q|2\mathbf{a}_2 - \mathbf{a}_1|)$, with $(p,q) = (19,11)$, $\mathbf{a}_1 = a\hat{\mathbf{e}}_x$, $2\mathbf{a}_2 = a(\hat{\mathbf{e}}_x + \sqrt{3}\hat{\mathbf{e}}_y)$, $a = 2.52$ Å the equilibrium lattice parameter of graphane, and $\hat{\mathbf{e}}_{x,y}$ the Cartesian unit vectors.

In order to test the accuracy of DF-TB results, we also calculate the smaller dots up to size $n \leq 24$ using density functional theory (DFT) in conjunction with all-electron projector augmented wave potentials[28,29] and the Perdew−Burke−Ernzerhof[30] generalized gradient approximation to the electronic exchange and correlation, as implemented in the VASP package.[31,32] In all of the cluster calculations, the Brillouin zone is represented by the Γ point. A well converged Monkhorst−Pack **k**-point set ($2 \times 2 \times 1$) is used for the array of QDs. Conjugate gradient scheme was employed to optimize the geometries until the forces on every atom were ≤0.05 eV/Å. The DF-TB calculated lattice parameters of graphene and graphane are 2.47 and 2.52 Å, respectively, in good agreement with the DFT values of 2.47 and 2.54 Å. In the DFT calculations, graphane is represented by a finite $C_{54}H_{72}$ cluster. The outermost C atoms are passivated by two H atoms, and these $>CH_2$ groups are kept frozen during geometry optimization to mimic the sp^3 C of infinite graphane. Periodic images are decoupled in normal direction by a vacuum space of ≃15 Å.

Acknowledgment. This work was funded by the Office of Naval Research. Computations were performed at the Department of Defense Supercomputing Resource Center at the Air Force Research Laboratory.

Note added in proof: After the completion of this work, a new experimental evidence of graphene hydrogenation has been reported,[33] further supporting the feasibility of patterning discussed above.

REFERENCES AND NOTES

1. Chakraborty, T. *Quantum Dots*; Elsevier: Amsterdam, 1999.
2. Novoselov, K. S.; Geim, A. K.; Morozov, S. V.; Jiang, D.; Zhang, Y.; Dubonos, S. V.; Grigorieva, I. V.; Firsov, A. A. Electric Field Effect in Atomically Thin Carbon Films. *Science* **2004**, *306*, 666–669.
3. Castro Neto, A. H.; Guinea, F.; Peres, N. M. R.; Novoselov, K. S.; Geim, A. K. The Electronic Properties of Graphene. *Rev. Mod. Phys.* **2009**, *81*, 109–162.

4. Han, M. Y.; Özyilmaz, B.; Zhang, Y.; Kim, P. Energy Band-Gap Engineering of Graphene Nanoribbons. *Phys. Rev. Lett.* **2007**, *98*, 206805.
5. Stampfer, C.; Schurtenberger, E.; Molitor, F.; Güttinger, J.; Ihn, T.; Ensslin, K. Tunable Graphene Single Electron Transistor. *Nano Lett.* **2008**, *8*, 2378–2383.
6. Ponomarenko, L. A.; Schedin, F.; Katsnelson, M. I.; Yang, R.; Hill, E. W.; Novoselov, K. S.; Geim, A. K. Chaotic Dirac Billiard in Graphene Quantum Dots. *Science* **2008**, *320*, 356–358.
7. Ritter, K. A.; Lyding, J. W. The Influence of Edge Structure on the Electronic Properties of Graphene Quantum Dots and Nanoribbons. *Nat. Mater.* **2009**, *8*, 235–242.
8. Matulis, A.; Peeters, F. M. Quasibound States of Quantum Dots in Single and Bilayer Graphene. *Phys. Rev. B* **2008**, *77*, 115423.
9. Recher, P.; Nilsson, J.; Burkard, G.; Trauzettel, B. Bound States and Magnetic Field Induced Valley Splitting in Gate-Tunable Graphene Quantum Dots. *Phys. Rev. B* **2009**, *79*, 085407.
10. Trauzettel, B.; Bulaev, D. V.; Loss, D.; Burkard, G. Spin Qubits in Graphene Quantum Dots. *Nat. Phys.* **2007**, *3*, 192–196.
11. Bets, K.; Yakobson, B. I. Spontaneous Twist and Intrinsic Instabilities of Pristine Graphene Nanoribbons. *Nano Res.* **2009**, *2*, 161–166.
12. Singh, A. K.; Yakobson, B. I. Electronics and Magnetism of Patterned Graphene Nanoroads. *Nano Lett.* **2009**, *9*, 1540–1543.
13. Sluiter, M. H. F.; Kawazoe, Y. Cluster Expansion Method for Adsorption: Application to Hydrogen Chemisorption on Graphene. *Phys. Rev. B* **2003**, *68*, 085410.
14. Sofo, J. O.; Chaudhari, A. S.; Barber, G. D. Graphane: A Two-Dimensional Hydrocarbon. *Phys. Rev. B* **2007**, *75*, 153401.
15. Muñoz, E.; Singh, A. K.; Ribas, M. A.; Penev, E. S.; Yakobson, B. I. The Ultimate Diamond Slab: GraphAne *versus* GraphEne. *Diamond Relat. Mater.* **2010**, *19*, 368–373.
16. Lebègue, S.; Klintenberg, M.; Eriksson, O.; Katsnelson, M. I. Accurate Electronic Band Gap of Pure and Functionalized Graphane from GW Calculations. *Phys. Rev. B* **2009**, *79*, 245117.
17. Nikitin, A.; Ogasawara, H.; Mann, D.; Denecke, R.; Zhang, Z.; Dai, H.; Cho, K.; Nilsson, A. Hydrogenation of Single-Walled Carbon Nanotubes. *Phys. Rev. Lett.* **2005**, *95*, 225507.
18. Ryu, S.; Han, M. Y.; Maultzsch, J.; Heinz, T. F.; Kim, P.; Steigerwald, M. L.; Brus, L. E. Reversible Basal Plane Hydrogenation of Graphene. *Nano Lett.* **2008**, *8*, 4597–4602.
19. Elias, D. C.; Nair, R. R.; Mohiuddin, T. M. G.; Morozov, S. V.; Blake, P.; Halsall, M. P.; Ferrari, A. C.; Boukhvalov, D. W.; Katsnelson, M. I.; Geim, A. K.; *et al.* Control of Graphene's Properties by Reversible Hydrogenation: Evidence for Graphane. *Science* **2009**, *323*, 610–613.
20. Lin, Y.; Ding, F.; Yakobson, B. I. Hydrogen Storage by Spillover on Graphene as a Phase Nucleation Process. *Phys. Rev. B* **2008**, *78*, 041402.
21. Berry, M. V.; Mondragon, R. J. Neutrino Billiards: Time-Reversal Symmetry-Breaking without Magnetic Fields. *Proc. R. Soc. London, Ser. A* **1987**, *412*, 53–74.
22. Dewar, M. J. S.; Dougherty, R. C. *The PMO Theory of Organic Chemistry*; Plenum: New York, 1975.
23. Herring, C. Some Theorems on the Free Energies of Crystal Surfaces. *Phys. Rev.* **1951**, *82*, 87–93.
24. Zhao, Y.; Yakobson, B. I. What is the Ground-State Structure of the Thinnest Si Nanowires? *Phys. Rev. Lett.* **2003**, *91*, 035501.
25. Sessi, P.; Guest, J. R.; Bode, M.; Guisinger, N. P. Patterning Graphene at the Nanometer Scale *via* Hydrogen Desorption. *Nano Lett.* **2009**, *9*, 4343–4347.
26. Aradi, B.; Hourahine, B.; Frauenheim, T. DFTB+, a Sparse Matrix-Based Implementation of the DFTB Method. *J. Phys. Chem. A* **2007**, *111*, 5678–5684.
27. Köhler, C.; Frauenheim, T. Molecular Dynamics Simulations of CF_x ($x = 2,3$) Molecules at Si_3N_4 and SiO_2 Surfaces. *Surf. Sci.* **2006**, *600*, 453–460.
28. Blöchl, P. E. Projector Augmented-Wave Method. *Phys. Rev. B* **1994**, *50*, 17953–17979.
29. Kresse, G.; Joubert, D. From Ultrasoft Pseudopotentials to the Projector Augmented-Wave Method. *Phys. Rev. B* **1999**, *59*, 1758–1775.
30. Perdew, J. P.; Burke, K.; Ernzerhof, M. Generalized Gradient Approximation Made Simple. *Phys. Rev. Lett.* **1996**, *77*, 3865–3868.
31. Kresse, G.; Furthmüller, J. Efficient Iterative Schemes for *Ab Initio* Total-Energy Calculations Using a Plane-Wave Basis Set. *Phys. Rev. B* **1996**, *54*, 11169–11186.
32. Kresse, G.; Hafner, J. *Ab Initio* Molecular Dynamics for Liquid Metals. *Phys. Rev. B* **1993**, *47*, 558–561.
33. Balog, R.; Jørgensen, B.; Nilsson, L.; Andersen, M.; Rienks, E.; Bianchi, M.; Fanetti, M.; Lægsgaard, E.; Baraldi, A.; Lizzit, S.; *et al.* Bandgap Opening in Graphene Induced by Patterned Hydrogen Adsorption. *Nat. Mater.* **2010**, *9*, 315–319.